COO-3158-61

AN IN-SITU FIELD-ION MICROSCOPE STUDY OF THE RECOVERY BEHAVIOR OF ION-IRRADIATED TUNGSTEN AND TUNGSTEN ALLOYS

by

Kenneth L. Wilson, Michael I. Baskes and David N. Seidman

Cornell University
Ithaca, New York 14853

April 1979

Report #4055

Prepared for

THE U.S. DEPARTMENT OF ENERGY UNDER
CONTRACT NO. EY-76-S-02-3158.*000.

DISCLAIMER

2024000

AN IN-SITU FIELD-ION MICROSCOPE STUDY OF THE RECOVERY BEHAVIOR OF ION-IRRADIATED TUNGSTEN AND TUNGSTEN ALLOYS*

K. L. Wilson and M. I. Baskes
Sandia Laboratories
Livermore, California 94550

D. N. Seidman
Cornell University, Bard Hall,
Department of Materials Science and Engineering
and the Materials Science Center
Ithaca, New York 14853

ABSTRACT

Five grades of tungsten specimens with different purity levels (resistivity ratios R of 5×10^4, 1.5×10^4, 50, 15, and 5) were irradiated in-situ with 30 keV W^+ ions to a dose of typically 5×10^{12} ion cm^{-2} at 18 K. Examination with a low-temperature field-ion microscope (FIM) showed the isochronal-annealing spectra of the specimens to result from a large self-interstitial atom (SIA) flux at ~38 K, followed by significant SIA flux from ~50 to 80 K and a small amount of additional recovery up to 120 K. The spectra for these five different R value specimens were essentially identical between 18 and 120 K. High-purity W specimens ($R = 5\times10^4$) doped with 5×10^{-5} to 1×10^{-4} atom fraction carbon showed only a small reduction in the amount

---

* Research supported by the United States Department of Energy. Additional support was received from the National Science Foundation through the use of the technical facilities of the Materials Science Center at Cornell University.

of recovery observed for the long-range migration peak at 38 K. The isochronal recovery spectra for tungsten-rhenium alloy specimens ($5x10^{-3}$ and $3x10^{-2}$ atom fraction Re) were radically different from the isochronal recovery spectra of pure W specimens. For both alloys the recovery of the Stage I long-range migration peak at 38 K was strongly suppressed; for the $3x10^{-2}$ atom fraction alloy, all recovery from 18 to 120K was virtually eliminated. This result indicated that during the long-range migration substage at 38 K tightly-bound, immobile SIA-Re complexes were formed that suppressed the SIA-SIA reaction. However, this effect was only observed at these high Re atom concentrations. The lack of any significant differences for the annealing spectra of the five purity-levels of undoped tungsten and the appearance of impurity effects only in the extremely concentrated tungsten alloys (i.e., $5x10^{-3}$ to $3x10^{-2}$ atom fraction Re) indicated that the early Stage II recovery (45 to 120 K) observed in the FIM isochronal-annealing spectra of self-ion irradiated high-purity tungsten was intrinsic in nature. Because of the highly inhomogeneous SIA distribution of the W^+ ion damage, the SIA-SIA interaction during Stage I long-range migration at 38 K appeared to be the dominant trapping mechanism. The early Stage II SIA recovery was therefore attributed to the migration or dissolution of these SIA clusters.

1. Introduction

The study of the recovery behavior of radiation damage in the refractory b.c.c. metals has received increasing attention over the past few years because of their potential importance in advanced energy systems. Of particular interest is the Stage II isochronal recovery of metals, which begins after the uncorrelated long-range migration of the self-interstitial atom (SIA) (typically at temperatures below 100 K) and continues until the prominent Stage III recovery peak at ~0.2 of the absolute melting temperature.[1] The Stage II recovery has been attributed to both extrinsic and intrinsic mechanisms. The interaction of SIAs with solute impurity atoms, in Stage II, has been studied in a number of irradiated f.c.c. alloys[2-17] and b.c.c. alloys.[18-22] On the other hand, there is also evidence for intrinsic behavior in Stage II involving SIA cluster growth.[23-26] In addition, complex extended SIA configurations have been proposed [27,28] for b.c.c. irradiated metals. The experimental research program reported in this paper was aimed at determining whether the Stage II isochronal recovery for tungsten was an intrinsic (i.e., involving only SIA-SIA interactions) or extrinsic (i.e., involving impurity atoms) phenomenon.

Since Thompson's[29] pioneering recovery experiments on neutron-irradiated tungsten there have been a number of other experiments on the isochronal-recovery behavior of thermal or fast-neutron irradiated tungsten (Burger et al.,[22] Coltman et al.,[30] and Takamura et al.[31]) employing electrical-resistivity measurements. In addition, there have been several experiments on the isochronal-recovery behavior of electron-irradiated tungsten (Neeley et al.,[32] Kunz,[33] Kunz

et al.,[34] Dausinger and Schultz[35] and Maury et al.[36]) also employing electrical-resistivity measurements. Dausinger and Schultz[35] have assigned the 38 K recovery peak, discussed in this paper, to close-pair recovery, while Maury et al.[36] have attributed it to the correlated recombination of freely migrating SIAs. Recently there have been a number of experiments on the isochronal-recovery behavior of electron, neutron, and proton or deuteron-irradiated tungsten (DiCarlo et al.,[37] Okuda and Mizubayashi,[38,39] and Townsend et al.[40]) employing internal-friction and dynamic-modulus measurements. In all of the above research on tungsten there has been the suggestion that impurity atoms may have played an exceedingly important role in the Stage II recovery. Thus, in the present work, the experimental emphasis was on the determination of the role, if any, played by impurity atoms on the isochronal-recovery behavior of ion-irradiated tungsten. Our experiment used the field-ion microscope (FIM) technique to observe Stage II recovery on an atomic scale.

The FIM technique[41] offers a unique atomistic view of the spatial arrangement and recovery behavior of point defects, introduced by radiation damage, in metals. When an FIM specimen is pulse field-evaporated, the lattice is dissected on an atom-by-atom basis: in this way the spatial arrangement of self-interstitial atoms (SIAs) and vacancies in the primary state of radiation damage is directly determined.[42] Alternatively when a specimen is irradiated at a low temperature (e.g., 10 K) and then warmed isochronally, the SIA flux to the free surface can be directly observed.[43,44] Prior FIM research on the isochronal recovery of self-ion irradiated tungsten[45-48] demonstrated that the SIA flux consisted of a large recovery peak centered at ~38 K; this peak

was followed by a significant amount of SIA recovery between 45 and 120 K. Our research on 20 or 30 keV W^+ ion-irradiated tungsten demonstrated that the long-range migration of an SIA occurs below 50 K; the SIA flux observed above this temperature was classified as Stage II recovery.

The FIM experiments consisted of irradiating with 30 keV W^+ ions, in situ five different purity levels of pure tungsten with 30 keV W^+ ions, tungsten alloys [W(C) and W(Re)] at an irradiation temperature, T_i, below the onset of long-range migration of the single SIA. Isochronal warming experiments to 120 K showed that all five different purity level of tungsten (resistivity ratio = 5 to $5x10^4$) had essentially the same basic recovery spectrum. Whereas the four W(C) and W(Re) alloys exhibited a reduction in the total amount of long range recovery; this effect was particularly strong for the W-$3x10^{-2}$ atom fraction (at. fr.) Re alloy. The reduced recovery observed in the tungsten alloys is readily understood in terms of the formation of tightly bound SIA-impurity atom complexes. However, these effects were only observed at extremely high impurity-concentrations not found in the five different purity levels of the unalloyed tungsten that were studied. We therefore concluded that the SIA recovery observed by FIM between 45 and 120 K in pure tungsten was intrinsic in nature, and we attributed the recovery to the migration and/or dissolution of SIA clusters formed at ~38 K during the single SIA long-range migration process.

2. Experimental Detail

2.1 Materials employed

The following five different purity-levels of tungsten and four tungsten alloys were investigated:

(1) four-pass zone-refined single crystals (R=5x10^4);

(2) one-pass zone-refined single crystals (R=1.5x10^4);

(3) Westinghouse polycrystalline wire annealed at 2400°C for one hour in a vacuum system which was at < 1x10^{-5} torr (R=50);

(4) Materials Research Corporation (MRC) VP-grade wire (R=15);

(5) Westinghouse polycrystalline wire in the as-received state (R=5);

(6) four-pass zone-refined single crystals doped with 50 appm carbon in solid solution;

(7) Westinghouse polycrystalline wire doped with carbon in solid solution;

(8) a commercial tungsten-5x10^{-3} at. fr. Re alloy; and

(9) a commercial tungsten-3x10^{-2} at. fr. Re alloy.

The zone-refined single-crystals were grown from both ~1 and 1.6 mm diameter rods of commercial purity tungsten.

Two standard physical measurements were employed to determine the purity of these specimens. The first technique employed was chemical analysis in the form of spark-source mass-spectrometry (SSMS).* This technique gave us the chemical composition of the metallic elements present in the specimen; however, SMSS did not distinguish between impurity atoms which were in solid solution and those which were in clusters or precipitates. Interstitial impurity-atom concentrations were measured by standard quantitative analysis techniques (e.g., the inert gas-fusion technique for carbon), but again there was no determination of the location of the impurity element.

* The SSMS technique is only good to within an order of magnitude unless reference standards are used for each specific element in question. Reference standards were not available for tungsten when the analyses of our specimens were performed. The SSMS measurements were performed in the Chemical Analytical Facility of the Cornell Materials Science Center.

The second measurement of specimen purity was the resistivity ratio $[R=\rho_{273\ K}/\rho_{4.2\ K}]$.* The value of $\rho_{4.2\ K}$ is sensitive to the total impurity atom concentration in solid solution. Unfortunately, R also does not provide any information on which impurity atoms were in solid solution. The tabulated values [45] of the specific resistivities of impurity atoms in tungsten indicated that a reasonable average value to use was $\approx 1\times10^{-6}$ Ωcm(at.%)$^{-1}$, although Dausinger et al.[50] have employed a value as low as 0.2×10^{-6} Ωcm(at.%)$^{-1}$ for molybdenum in tungsten.

Tables I and II summarize the results of the chemical analyses and the R data for the different specimens employed in this study. The value $R\approx5\times10^{4}$ corresponds to $\sim10^{-6}$ at. fr. impurity atoms, while $R\approx5$ corresponds to an impurity atom concentration of $\lesssim 10^{-2}$ at. fr. based on 1×10^{-6} Ωcm(at.%)$^{-1}$ as the average specific resistivity of an impurity atom. It is clear from a comparison of Tables I and II that the chemical analyses and R data are <u>not</u> in agreement. This is indicative of the fact that the concentration of impurity atoms in solid solution must have been quite different from the total impurity-atom concentration in each specimen.

2.2. Preparation of tungsten-(carbon) alloys

Both four-pass zone-refined and Westinghouse annealed tungsten wire were doped with carbon** by a quenching technique similar to the one described by Krautz et al.[52] The single-crystal tungsten specimen, which was quenched, was first electropolished to a

---

* The value of $\rho_{273\ K}$ has been taken to be equal to 4.95×10^{-6} Ωcm.[49]

**Carbon is an interstitial impurity atom in tungsten with an extremely small solid-solubility; the solubility of carbon in tungsten appears to to be $\lesssim 5\times10^{-3}$ at. fr. at 2475°C.[51].

diameter of 0.2 mm; next, it was suspended vertically in a vacuum chamber which was backfilled to a partial pressure of 1×10^{-4} torr methane. The electrical and thermal contacts to the specimen were made by clamping the specimen at its top end and immersing the bottom end in a liquid ternary-eutectic of gallium, indium and tin which has a melting point of 10°C (United Mineral and Chemical Corp., alloy UG-1). The specimen was resistively heated to 1500°C for a period of 4 h and then radiation quenched by terminating the current. An annealed Westinghouse tungsten wire of 0.125 mm diameter was quenched in a similar manner after having been equilibrated for 4 h at 2000°C in 10^{-4} torr methane.

In the case of the four-pass zone-refined tungsten specimen the value of R was $\simeq 250$ after the quench. The only available value for the resistivity of a carbon atom in solid solution in W is 3.85×10^{-6} Ωcm(at.%)$^{-1}$;[52] therefore, on the basis of this value the single crystal contained ~50 appm carbon. The carbon concentration in solid solution in the polycrystalline wire could not be established quantitatively. The wire was quenched from a higher temperature and at a faster quenching rate* than was the single crystal; the grain boundaries in the wire specimen certainly allowed for the possibility of segregation of the rapidly diffusing carbon** atoms. The end result was that the polycrystalline wire was extremely brittle after this carbon-doping treatment.

---

* The quenching rate of a wire due to radiation cooling is inversely proportional to its diameter.

** The diffusivity of a carbon atom in a tungsten lattice is given[53] by $(3.4 \times 10^{-3}\ \text{cm}^2\text{sec}^{-1})\exp(-1.6\ \text{eV}/kT)$.

2.3 The isochronal-recovery experiment

The basic experimental FIM procedures have been described elsewhere.[43-47] Briefly, the specimens were electropolished, field evaporated to a useful tip radius (200-400 Å) and then irradiated with 30 keV W^+ at 18 K in the FIM in the absence of the imaging gas or the electric field.* Typical fluences were ~5×10^{12} W^+ cm^{-2}. After each irradiation, the specimen was re-imaged and pulse field-evaporated; a minimum of 5 Å of metal was removed by this technique. Then the temperature of the specimen was increased at a rate of ~2.5 K min^{-1}, while the FIM image was recorded on 35 mm cine film at 0.5 frame $(sec)^{-1}$. The arrival of SIAs at the surface was detected by the appearance of extra bright-spots.[43-45,47,17] The flux of these extra bright-spots was correlated with specimen temperature; thereby, producing an isochronal recovery spectrum for SIA recovery.

3. RESULTS

3.1 The isochronal-recovery behavior of the pure tungsten.

The isochronal-recovery spectra** for the one-pass zone-refined (R=1.5×10^3), annealed Westinghouse (R=50), the MRC VP-grade (R=15), and the Westinghouse as-received tungsten (R=5), are presented in Figures 1 to 4 respectively. The spectrum for the four-pass zone-refined (R=5×10^4)

---

* At 18 K there was no long-range migration of the SIA.[45, 48] Recently we have repeated these experiments at 20 K employing 30 keV W^+ ions and reconfirmed the fact that SIAs were not mobile at this temperature.

**The histograms exhibited in this section were constructed from the superposition of several runs; a maximum of three irradiations was performed on each tip. From 100 to 1000 Å of metal was removed between each irradiation to increase the bluntness of the tip. In order to ascertain the effect of re-irradiating a given specimen two runs were made on the same crystal with only 5 Å of metal removed between the two irradiations. No large changes were found in the isochronal-annealing spectra, indicating that the depleted-zone distribution and density did not play a major role in the observed recovery behavior. Table III summarizes the relevant data for all the isochronal anneals performed.

had been previously presented [see Figure 2(A) of reference 47]. The histograms show the fraction of SIA defects per 5 K interval as a function of T in the range 18 to 120 K for specimens that had been irradiated with 30 keV W^+ ions at 18 K in the absence of the imaging field. These four different grades (i.e., R=5x10^4 to 15) of W displayed remarkably similar annealing spectra. The 38 K long-range migration peak was the dominant feature in all four cases. Three possible recovery peaks were found at ~50, 60 and 80 K and an extremely ill-defined tail which might contain additional peaks at 95 and 110 K was also observed. The fifth grade of tungsten studied was Westinghouse wire in the as-received unannealed state (R=5). The isochronal spectrum (see Figure 4) lacked the sharp peak structure found in the purer specimens, but the dominant 38 K peak was still present. Hence, the value of R for pure tungsten was varied by a factor of 10^4 and yet the basic annealing spectrum had not shown any significant change.

The insensitivity of the observed recovery spectra to the value of R was a somewhat surprising result. A possible explanation of this result is based on the following observations concerning the MRC-VP grade tungsten: (1) the grain size or subgrain size has been found to be very small, i.e., many grain boundaries have been detected, by the FIM technique, in the unannealed MRC-VP grade tungsten specimens examined at Cornell; and (2) unpublished (A. Wagner, J. Amano and D. N. Seidman) atom-probe FIM studies, at Cornell, of unannealed MRC-VP grade tungsten revealed a total impurity-concentration of $<<10^{-4}$ at. fr. in the interior of the grains. Thus the R value may have been determined by electron scattering from impurity atoms which had segregated to the subgrain boundaries or

from the grain boundaries themselves.*

3.2 The isochronal-annealing spectra of W(C) alloys

Figure 5 exhibits the isochronal annealing spectrum of the four-pass zone-refined W with ~5×10^{-5} at. fr. of carbon in solid solution. The Stage I long-range migration peak at 38 K had diminished only slightly in size. The isochronal annealing spectrum of the Westinghouse W doped with carbon (Figure 6) also showed only a small effect. Thus, while the carbon level in solid solution in the four-pass zone-refined W ($R\approx5\times10^{4}$) was increased by a factor of ~200 over its concentration in the undoped single crystals, the effect on the isochronal annealing spectrum was small. We stress that these high carbon concentrations are not found in the undoped tungsten specimens.

3.3 The isochronal-recovery behavior of W(Re) alloys

The five grades of W used for the studies presented in Section III each contained less than 10^{-5} at. fr. Re (see Table I). The isochronal-annealing spectra of the irradiated W-0.5×10^{-3} at. fr. Re (5×10^{3} appm) and W-3×10^{-2} at. fr. Re alloys are presented in Figures 7(A) and 7(B). In Figure 7 the ordinate is given as the number of SIAs per 5 K interval because of the small number of SIA events observed.

In the case of the W-5×10^{-3} at. fr. Re alloy the long-range migration peak temperature was between 30 and 35 K, instead of 35-40 K, as in the case of the undoped W specimens. This shift is easily explained if one considers that only the SIAs close to the surface could have reached the surface without having been trapped by Re atoms. These SIAs would

---

* The above observations and comments are consistent with the lack of agreement between the R values and the chemical analyses presented in Section 2.1.

have constituted the early part of the flux because of the short diffusion distance to the surface. This downward shift in peak temperature with increasing impurity atom-concentration had been predicted by the Seidman and Lie treatment of this diffusion problem (see Figure 6 in Reference 43). The substage II_A peak at 50 K has now become the dominant peak, while recovery from 60 to 80 K has almost vanished. In addition, there was an increase in the amount of recovery above 90 K.

The W-$3x10^{-2}$ at. fr. Re alloy showed almost no recovery over the entire range from 18 to 120 K. The recovery peak at 110 K was the largest one, but it contained only three SIAs after a total of six recovery experiments; therefore, for both of these alloys there is strong evidence that the SIAs formed SIA-Re atom complexes in Stage I. In the case of the W-$3x10^{-2}$ at. fr. Re alloy the fraction of the Stage I SIAs trapped was appreciable since the 38 K peak was essentially eliminated,* as were all the Stage II peaks below 120 K. The lack of a significant SIA flux below 120 K indicated that a SIA-Re atom complex has a dissociation enthalpy of $\gtrsim$ 0.3 eV** in the W-$3x10^{-2}$ at. fr. Re alloys. Further experimental work on this problem [Nielsen[56] and Nielsen and Seidman[57]] indicated that the lower limit of the binding enthalpy of an SIA to a rhenium atom is ~0.8 eV.**

---

* This suppression of the SIA long-range migration recovery-peak has also been observed for a number of f.c.c. alloys (e.g., see Sosin and Neely[54], Sosin[4], and Schilling et al.[55]).

** Calculated by assuming that the binding plus motion enthalpy (i.e., the dissociation enthalpy) is proportional to the peak temperature;[4] i.e., the dissociation enthalpy scales linearly with temperature.[4,17]

3.4. SIA contrast patterns detected during isochronal anneals

The primary SIA contrast pattern observed during the isochronal warming experiments was a single extra-atom spot.* Amongst the 1062 SIA events observed in the isochronal annealing experiments (see Section 4.A) 91.25% exhibited this simple contrast pattern; a double-spot contrast pattern was observed in 6.68% of the total number of events; and the remaining 2.07% of the SIA events were multiple-spot contrast patterns** with three or more extra-atom spots. Figure 8 gives some examples of these contrast effects.

The single-spot contrast effect could have arisen from an atom on the surface (an adatom created by the total relaxation of an SIA at the surface) or by a surface or a subsurface atom that was displaced upward as a result of an SIA lying several atomic-layers below the specimen's surface (Seidman and Lie[58]). The double-spot contrast pattern may have had two distinct origins. First, the contrast model of Seidman and Lie[58] predicted that for certain orientations the <110> split SIA can produce a double-spot contrast effect at the surface: this model requires that the SIA retains its identity as a subsurface defect. Second, the double-spot contrast pattern could indicate the arrival of a di-SIA complex at the surface. Analysis of the double-spot contrast patterns in all of the unalloyed tungsten specimens showed that the double-spot contrast effects occurred over the entire temperature range in which single-spot contrast effects were observed. The coexistence of single and double-spot contrast effects in the 38 K long-range migration peak indicated that both

* This contrast pattern has also been referred to as an extra bright-spot by a number of authors, including the present ones.

** A multiple-spot contrast pattern was considered as a single SIA event in the construction of the isochronal-annealing histograms; hence, the use of the term defects in labeling the ordinates.

contrast effects had the same origin: that is, the single SIA. Therefore, a reasonable conclusion is that at least some of the SIA contrast effects were caused by the strain field of a subsurface SIA. Whether this mechanism was the only one that was operative cannot be ascertained at present.

Contrast patterns with three or more spots (see the pairs of FIM micrographs E and F, and G and H in Figure 8) were much larger in extent than the predicted strain field contrast effect patterns of Seidman and Lie[58] for the single SIA. While these events were only a small portion (~2%) of the total number of defects detected their appearance indicated that some form of SIA clustering must have occurred within the FIM specimen during the isochronal anneals. Because of the small number of multiple contrast patterns it was not clear if their migration enthalpy was possibly lowered by a large negative $p\Delta v_{ic}^{m}$ effect; where Δv_{ic}^{m} is the volume change of migration of the SIA cluster and p is the hydrostatic pressure due to the applied electric imaging field. With respect to the latter point the 100 K irradiation experiment of Scanlan et al.[45] and the 50 K irradiations by Wilson and Seidman [47] showed that the single-spot peak structure observed below 100 K in the isochronal anneals was <u>not</u> assisted by the electric field: their experiment do not rule out a $p\Delta v_{ic}^{m}$ effect for the SIA clusters. In fact, the three SIA events detected in the isochronal recovery below T_i=100 K in the Scanlan et al.[45] experiment were multiple-spot contrast effects.

Control experiments

Six control-runs were performed during the course of the isochronal annealing experiments. Three of the specimens were simply annealed

from 18 to 120 K without being irradiated, while the other three specimens had been irradiated, but had flashed* during the post-irradiation peel prior to the isochronal anneal.

One contrast pattern similar to an SIA was observed in the first control-run on an unirradiated specimen; no SIA contrast effects were observed in any of the subsequent control runs. This single contrast effect in these controls may have been caused by a gas impurity-atom that had been adsorbed on the surface. The high electric field required for field ionization of helium kept impurity adsorption to a minimum.[41d] In one of the control runs, the specimen was exposed to the ion accelerator (at $\sim 10^{-5}$ torr argon gauge pressure) without the differential pumping system for ~30 minutes. No SIA contrast effects were observed in the subsequent control anneal from 18 to 120 K. If the six control-specimens had been irradiated at 18 K and annealed in the standard way there would have been ~150 SIA events detected.** Therefore an upper maximum to the gas impurity contamination effect was $\lesssim$0.7% for the isochronal anneals. This background was <u>insignificant</u> with respect to the SIA flux observed in the isochronal anneals reported in this paper.

4. Major Experimental Results and Discussion

The major experimental results are summarized as follows:

(1) The low-temperature isochronal-annealing spectrum of pure tungsten ($R=5\times10^4$), irradiated <u>in-situ</u> with 30 keV W^+ ions to a typical

---

* Flashing is a common mode of tip failure whereby a shell of material is expelled from the surface. The tip can still be imaged at a higher voltage, but the SIAs have most likely been swept out of the tip volume: see Wilkes et. al.[59] and Loberg[60] for more details on tip failure.

** This number was calculated for 30 keV W^+ ions for a dose of 5×10^{12} ion cm^{-2} assuming approximately one observable SIA per incident ion: this number is borne out by our experimental results.

fluence of ~5×10^{12} cm^{-2} at 18 K was shown to consist of a series of distinct recovery peaks at ~38, 50, 65 and 80 K with a small amount of additional recovery observed up to 120 K. We had previously identified the 38 K peak as an SIA long-range migration substage. The remaining peaks were classified as substages of Stage II; therefore, Stage II of irradiated tungsten begins at 45 K and <u>not</u> at ~100 K as had been suggested by earlier investigators (see Reference 44 for a discussion of this point).

(2) The isochronal annealing-spectrum of pure tungsten observed by FIM between 18 and 120 K was insensitive to R for values between 5×10^{4} and 5.

(3) Self-ion irradiated tungsten doped with ~5×10^{-5} to 1×10^{-4} at. fr. interstitial carbon, in solid solution, showed only a small reduction in the amount of recovery observed for the long-range migration peak at 38 K in undoped tungsten. However, SIA-carbon atom interactions <u>cannot</u> be invoked in the explanation of early Stage II recovery in the high-purity tungsten, since $R\cong5\times10^{4}$ corresponds to $\lesssim 2\times10^{-7}$ at. fr. carbon in solid solution.

(4) The isochronal-annealing spectra for self-ion irradiated tungsten-5×10^{-3} and 3×10^{-2} at. fr. rhenium alloys were radically different from the isochronal-recovery spectra of pure tungsten. For both tungsten (rhenium) alloys the amount of recovery for the long-range migration peak at ~38 K was suppressed and in the case of the W-3×10^{-2} at. fr. Re alloy all recovery between 18 and 120 K was almost completely eliminated. This result constitutes strong evidence for the formation of immobile tightly-bound SIA-rhenium complexes during the long-range migration substage at 38 K. However, these effects only became apparent at high Re concentrations. We stress again that in the high purity tungsten ($R\simeq5\times10^{4}$), the Re impurity concentration in solid solution was $\lesssim 10^{-5}$ at. fr.

(5) The SIA contrast patterns detected in the isochronal anneals consisted primarily of single extra-spots. However, the small number of large multiple-spots indicated that some form of SIA clustering must have occurred below 120 K in Stage II during the isochronal-annealing experiments.

The lack of any significant change in the recovery spectrum for samples with $R=5\times10^4$ to $R=5$, led us to the conclusion that for the unalloyed tungsten specimens the SIA-impurity interactions did not make any appreciable contribution to the Stage II SIA flux.* Instead, we propose that SIA-SIA interactions dominated the recovery behavior. This situation results from the inhomogeneous distribution of SIAs created by the 30 keV W^+ ions in the FIM specimen. Each heavy metal-ion produces a depleted zone which consists of a cloud of SIAs surrounding the vacancy-rich core.[42,43] Experiments performed by Beavan et al.[61] have shown that an irradiation temperature of 18 K a 20 keV W^+ ion in W can create a depleted zone consisting of ~160 vacancies surrounded by a significant number of SIAs within a ~100 Å radius. The SIA concentration within this cloud was as high as $\sim10^{-2}$ at. fr. and the average impurity-atom concentration in the 5×10^4 samples was $\lesssim10^{-6}$ at. fr.; therefore, the probability of an SIA-SIA interaction was several orders of magnitude greater than an SIA-impurity interaction. Recent experiments by Wei and Seidman [62] on tungsten irradiated, at 10 K, with 30 keV W^+, Mo^+ or Cr^+ ions have substantiated the physical picture detailed above.

In the case of the $R=15$ specimens the impurity-atom concentration in the interior of the subgrains was $<<10^{-4}$ at. fr. (see Section III.A) so

*We have found no evidence to support Okuda and Mizubayashi's[38,39] conclusion that the recovery at 30 K in neutron-irradiated tungsten was a result of the detrapping of SIAs from impurity atoms. It is noted that there is also a very fundamental disagreement between Townsend et al. [40] and Okuda and Mizubayashi[38,39] on the interpretation of the 30 K internal-friction peak.

that the migrating SIAs sampled a lattice which was considerably purer than a first-order interpretation of the R value would have lead us to believe. Furthermore it is also possible that the specific impurity atoms present in the impure tungsten do not form SIA-impurity atom complexes with the correct binding enthalpy to perturb the basic recovery spectrum. Once again, SIA-SIA interactions were more probable than SIA-impurity interactions.

These results should be contrasted with resistivity measurements on electron-irradiated metals: e.g., see references 4-9 and 32-36. In the case of electron-irradiated specimens the SIAs were distributed uniformly and at a low concentration relative to the concentration in the SIA cloud of the self-ion irradiated specimens. In addition, the mobile SIAs sampled many more lattice sites via random walk in the bulk electron-irradiated specimens than in the self-ion irradiated FIM specimen, because of the different SIA sink distribution.* Therefore, SIA-impurity interactions were prominent at a much lower impurity-atom concentration in the electron-irradiated bulk sample than in the self-ion irradiated FIM sample.

The Stage II SIA recovery flux observed by FIM from 45-120 K is therefore an intrinsic phenomenon for the pure tungsten specimens. We feel that it is caused by the long-range migration and/or dissolution of SIA complexes formed during the long-range migration in Stage I (38 K). Only when large quantities of specific impurity atoms (5×10^{-5} at. fr. C, 5×10^{-3} and 3×10^{-2} at. fr. Re) were introduced into solid solution did the basic FIM recovery spectrum exhibit significant changes. At these impurity levels the SIA-impurity atom interactions began to dominate over SIA-SIA

* An SIA will make $<10^4$ jumps before it reaches the external surface of the FIM specimen, while the number of jumps for an SIA to reach a vacancy, in an isochronal anneal of an electron-irradiated specimen, is inversely proportional to the vacancy concentration and therefore is usually $>10^4$.

interactions. The small decrease of the amount of recovery for the 38 K peak in the W(C) alloys, and the virtual elimination of Stages I and II in the W-$3x10^{-2}$ at. fr. Re alloys were indicative of the SIA capture cross-sections and dissociation enthalpies of the different SIA-impurity atom complexes.

In order to understand the experimental observations in a more quantitative fashion a diffusion model was constructed for the FIM Stage I isochronal recovery experiments. The following approximations were made in modeling the experiment: (1) the FIM tip was approximated by a sphere with a 300 Å radius; (2) the depleted zone produced by a single incident-ion was taken to be a 15 Å radius sphere whose center lay at the center of the spherical FIM tip; (3) the spherical depleted zone was surrounded by 100 SIAs at radii (r) greater than or equal to 40 Å; (4) the SIA distribution function was chosen arbitrarily to be proportional to r^{-1} with a maximum SIA concentration of $2x10^{-3}$ at. fr.; and (5) the impurity atoms were distributed uniformly between the outer and inner spherical surface. The coupled set of non-linear partial differential equations governing this situation were solved numerically; in order to obtain an isochronal recovery spectrum the specimen's temperature was increased in a linear fashion through Stage I. In this diffusion problem the SIAs were allowed to form immobile di-SIAs, immobile SIA-impurity atom complexes and to diffuse to either the outer or inner surface; the SIAs were <u>not</u> allowed to detrap below 50 K. The effects, on the Stage I recovery behavior, of impurity-atom concentrations ranging from 10^{-6} to 10^{-1} at. fr. were determined. Further details concerning this model can be found in the Appendix.

The results of these calculations are exhibited in Figure 9. This figure shows, as a function of the impurity-atom concentration: (1) the fraction of SIAs that form di-SIAs; (2) the fraction of SIAs that become trapped at impurity atoms; and (3) the fraction of SIAs that escape to the outer surface (r=300 Å) during Stage I. The fraction of SIAs that arrive at the depleted zone surface is omitted from Figure 9. The numerical values are, of course, sensitive to factors such as the SIA distribution function and tip geometry; nevertheless, the results indicate the qualitative trends in the competition between di-SIA formation and impurity-atom trapping. For low impurity-atom concentrations ($\sim 10^{-6}$ to 10^{-5} at. fr.) di-SIA formation dominates the internal trapping possibilities. This impurity-atom regime includes the pure tungsten specimen with $R = 5 \times 10^{4}$ to 15. At $\sim 10^{-4}$ at. fr., di-SIA formation is still significantly greater than impurity atom trapping, but the Stage I SIA flux to the surface is diminished as impurity atoms begin to trap mobile SIAs that would otherwise have reached the surface in the absence of impurity atoms. Therefore, as seen in the carbon-doped samples, Stage I decreases slightly in magnitude, but Stage II (45-120 K) is essentially unchanged because almost all of the trapped SIAs still reside in di-SIA clusters. Finally, for impurity-atom concentrations approaching $\sim 10^{-2}$ at. fr., impurity atom trapping became the dominant reaction. Virtually no SIAs reached the outer surface during Stage I, and in Stage II the SIA flux to the surface was controlled totally by SIA-impurity atom binding enthalpies. In the experiment with 3×10^{-2} at. fr. Re alloys, no significant recovery was observed below 120 K. The results of the diffusion model are therefore in good qualitative agreement with the FIM observations of SIA recovery in pure and alloyed tungsten.

In conclusion the early Stage II SIA recovery spectrum, observed by the FIM technique, for self-ion irradiated tungsten has been shown to be intrinsic in nature and has been attributed to the dissolution and/or migration of SIA complexes formed during the Stage I long-range SIA migration. SIA-impurity atom effects were shown to play a dominant role in the early Stage II recovery spectrum only at very high impurity-atom concentrations of the impurity rhenium. The importance of SIA-SIA interactions can be traced to the highly anisotropic spatial-distribution of SIAs in a 30 keV W^+ irradiated FIM specimen.

ACKNOWLEDGMENTS

The authors wish to thank Mr. B. F. Addis for his help in the preparation of the zone-refined single crystals of tungsten and the carbon-doped tungsten specimens, Mr. C. H. Nielsen for measuring the resistivity ratios of the tungsten-(rhenium) alloys, Mrs. K. Pratt for her aid in scanning ciné film and Mr. R. Whitmarsh for his general technical assistance.

Appendix

In this Appendix we give some details concerning the diffusion model discussed in Section IV. The inner and outer radii of the solid annular spherical volume are denoted r=a and r=b respectively. All SIA clusters of a size greater than a di-SIA were neglected and it was assumed that the impurity atom traps were unsaturable. Subject to all the assumptions and approximations stated, the set of coupled non-linear partial differential equations is:

$$\frac{\partial C_{1i}}{\partial t} = D_{1i}\left[\frac{\partial^2 C_{1i}}{\partial r^2} + \frac{2}{r}\frac{\partial C_{1i}}{\partial r}\right] - 2\,K_1\,C_{1i}^2 - K_2\,C_*\,C_{1i}; \tag{A1}$$

$$\frac{\partial C_{2i}}{\partial t} = K_1\,C_{1i}^2\ ;\ \text{and} \tag{A2}$$

$$\frac{\partial C_{*i}}{\partial t} = K_2\,C_*\,C_{1i}\ . \tag{A3}$$

The rate constants K_1 and K_2 and the SIA diffusion coefficient (D_{1i}) are given by the expressions:

$$K_1 = g_1\,\nu_{1i}\,\exp\left(-\Delta h_{1i}^m/kT\right); \tag{A4}$$

$$K_2 = g_2\,\nu_{1i}\,\exp\left(-\Delta h_{1i}^m/kT\right);\ \text{and} \tag{A5}$$

$$D_{1i} = g_3\,a_o^2\,\nu_{1i}\,\exp\left(-\Delta h_{1i}^m/kT\right). \tag{A6}$$

The quantities C_{1i}, C_{2i}, C_{*i}, and C_* are the concentrations of SIAs, di-SIA, SIA-impurity atom complexes, and impurity atoms respectively. The quantity

Δh^{III}_{1i} in the enthalpy change of migration of the SIA,* ν_{1i} is the frequency with which an SIA attacks the enthalpy barrier, g_1, g_2, and g_3 are geometric factors, and a_o is the lattice parameter. The Eqs. (A1) to (A3) were subjected to the initial conditions (t=o):

$$C_{1i} = f(r); \tag{A7a}$$

$$C_{2i} = 0; \text{ and} \tag{A7b}$$

$$C_{*i} = 0. \tag{A7c}$$

The boundary conditions were taken to be:

$$C_{1i}\,(r) = 0 \quad \text{at} \quad r=a; \text{ and} \tag{A8a}$$

$$C_{1i}\,(r) = 0 \quad \text{at} \quad r=b. \tag{A8b}$$

The expression for D_{1i} was taken from the work of Scanlan et al. [45,46]:

$$D_{1i} = 0.22 \exp\,(-0.085 \text{ eV/kT})\ \text{cm}^2\text{sec}^{-1}\ . \tag{A9}$$

The quantity g_1 is the number of ways a di-SIA can be formed from two single SIAs, g_2 is the number of ways an SIA-impurity atom cluster can form and g_3 is a diffusional factor which depends on the crystal lattice. The SIA was assumed to have the <110> split configuration in the b.c.c. tungsten lattice.[64] The di-SIA was assumed to consist of two parallel <110> split SIAs with their center-of-gravity located on two first nearest-neighbor sites.[65] With these assumptions we calculated g_1, g_2, and g_3 to be

*The entropy change of migration (Δs^m_{1i}) of an SIA has been taken to be equal to zero.

66, 10, and (1/6) respectively. The quantity ν_{1i} was calculated from Eqs. (A6) and (A9).

The SIAs were taken to be immobile initially at 18 K. The temperature of the specimen was then increased linearly with time (t) to the end of Stage I (45 K). The coupled set of nonlinear partial differential equations [Eqs. (A1) to (A3)] were solved numerically by first approximating each partial differential equation by N ordinary differential equations in time. A uniform set of 60 radial mesh points was used. The resulting system of 180 coupled ordinary differential equations was solved numerically using the Gear method.[66] The concentration profiles of the trapped SIAs were integrated over volume to yield the total number of SIAs trapped during Stage I. The flux of SIAs at the outer surface $-D_{1i} \left(\frac{\partial C_{1i}}{\partial r}\right)_{r = b}$ was integrated over time to yield the total number of SIAs that reached the outer surface during Stage I. These SIA totals are shown in Figure 9 as a function of the impurity atom-concentration.

REFERENCES

1. F. W. Young, Jr. J. Nucl. Mater. 69 & 70, 310 (1978).

2. T. H. Blewitt, R. R. Coltman, C. E. Klabunde and T. S. Noggle, J. Appl. Phys. 28, 639 (1957).

3. D. G. Martin, Phil. Mag. 6, 839 (1961); D. G. Martin, ibid. 7, 803 (1962).

4. A. Sosin, in Lattice Defects and Their Interactions, ed. by R. R. Hasiguti (Gordon and Breach, New York, 1967), pp. 235-266.

5. C. P. Cannon and A. Sosin, Rad. Effects 25, 253 (1975).

6. W. Schilling, K. Sonnenberg and H. J. Dibbert, Rad. Effects 16, 57 (1972).

7. H. Wollenberger, in Proceedings of Fundamental Aspects of Radiation Damage in Metals, edited by M. T. Robinson and F. W. Young, Jr. (National Technical Information Service, Springfield, Virginia, 1975), pp. 582-600.

8. H. Wollenberger, J. Nuc. Mater. 69 & 70, 361 (1978).

9. C. Dimitrov, in Proceedings of Fundamental Aspects of Radiation Damage in Metals, edited by M. T. Robinson and F. W. Young, Jr. (National Technical Information Service, Springfield, Virginia, 1975), pp. 608-14.

10. M. L. Swanson, L. M. Howe and A. F. Quennville, ibid. pp. 316-24.

11. M. L. Swanson and F. Maury, Can. J. Phys. 53, 1117 (1975); M. L. Swanson, Howe, L. M., and A. F. Quenneville, J. Nuc. Mater. 69 & 70, 372 (1978).

12. M. Kiritani, in Proceedings of Fundamental Aspects of Radiation Damage in Metals, edited by M. T. Robinson and F. W. Young, Jr. (National Technical Information Service, Springfield, Virginia, 1975), pp. 695-714.

13. K. Nakata, K. Ikeuchi, H. Hirano, K. Furukawa and J. Takamura, ibid. pp. 622-28.

14. W. Mansel, G. Vogl and W. Koch, Phys. Rev. Lett. 31, 359 (1973).

15. G. Vogl, J. de Phys. 35 C6-165 (1974).

16. G. Vogl, in Proceedings of Fundamental Aspects of Radiation Damage in Metals, edited by M. T. Robinson and F. W. Young, Jr. (National Technical Information Service, Springfield, Virginia, 1975), pp. 349-60.

17. C.-Y. Wei and D. N. Seidman, Rad. Effects 32, 229 (1977).

18. H. Wagenblast and A. C. Damask, J. Phys. Chem. Solids 23, 221 (1962).

19. M. Wuttig, J. T. Stanley and H. K. Birnbaum, Phys. Status Solidi 27, 701 (1968).

20. M. Weller and J. Diehl, Scripta Met. 10, 101 (1976).

21. K. Niebel and M. Wilkens, Phys. Status Solidi (a) 25 77 (1974).

22. G. Burger, K. Isebeck, R. Kerter, J. Völkl, H. Wenzl, H.-H. Kuhlmann and H. Schultz, Phys. Letters 20, 470 and 472 (1966).

23. A. Bourret, Phys. Status Solidi (a) 4, 813 (1971).

24. K. Urban and A. Seeger, Phil. Mag. 30, 1395 (1974).

25. P. Ehrhart and W. Schilling, Phys. Rev. B 8, 2604 (1973).

26. P. Ehrhart and U. Schlagheck, J. Phys. F: Metal Phys. 4, 1575 (1974); P. Ehrhart and U. Schlagheck, ibid. 4, 1589 (1974).

27. H. B. Afman, Phys. Status Solidi (a) 11, 705 (1972); H. B. Afman, in Proceedings of International Meeting on Defects in Refractory Metals, edited by R. deBatist, J. Nihoul and L. Staals (Studie Centrum voor Kernenergie/Centre d'Etude Nucleaire, Mol, Belgium, 1972), pp. 19-20.

28. P. Moser, ibid., pp. 65-7.

29. M. W. Thompson, Phil. Mag. 5, 278 (1960).

30. R. R. Coltman, C. E. Klabunde and J. K. Redman, Phys. Rev. 156, 715 (1967).

31. S. Takamura, R. Hanada, S. Okuda and H. Kimura, J. Phys. Soc. Japan 30, 1091 (1971).

32. H. H. Neely, D. W. Keefer and A. Sosin, Phys. Status Solidi 28, 675 (1968).

33. W. Kunz, Phys. Status Solidi (b) 48, 387 (1971).

34. W. Kunz, K. Faber, R. Lachenmann and H. Schultz, in Proceedings of the International Meeting on Defects in Refractory Metals, edited by R. deBatist, J. Nihoul and L. Staals (Studie Centrum voor Kernenergie/Centre d'Etude de L'Energie Nucleaire, Mol, Belgium, 1972), pp. 7-12.

35. F. Dausinger and H. Schultz, Phys. Rev. Lett. 35, 1773 (1975); F. Dausinger, Phil. Mag. A 37, 819 (1978).

36. F. Maury, M. Biget, P. Vajsa, A. Lucasson and P. Lucasson, Rad. Effects, 38, 53 (1978).

37. J. A. DiCarlo, C. L. Snead, Jr. and A. N. Goland, Phys. Rev. 178, 1059 (1969).

38. S. Okuda and H. Mizubayashi, Phys. Rev. Lett. 34, 815 (1975).

39. S. Okuda and H. Mizubayashi, Phys. Rev. B, 13, 4207 (1976).

40. J. R. Townsend, M. Schildcrout and C. Reft, Phys. Rev. B, 14, 500 (1976).

41. For reviews of the FIM technique and some of its applications see:

    (a) Field-Ion Microscopy, edited by J. J. Hren and S. Ranganathan (Plenum Press, New York, 1968);

    (b) E. W. Müller and T.-T. Tsong, Field-Ion Microscopy (American Elsevier, New York, 1969);

    (c) K. M. Bowkett and D. A. Smith, Field-Ion Microscopy (North-Holland, Amsterdam, 1970); and

    (d) E. W. Müller and T.-T. Tsong, in Progress in Surface Science, edited by S. G. Davison (Pergamon Press, Oxford, 1973), Vol. 4, Part 1, pp. 1-139.

    (e) J. A. Panitz, in Progress in Surface Science, edited by S. G. Davison (Pergamon Press, Oxford, 1978), Vol. 8, pp. 219-262.

42. D. N. Seidman, in Radiation Damage in Metals, edited by N. L. Peterson and S. D. Harkness (American Society for Metals, Metals Park, Ohio,1976), pp. 28-57.

43. D. N. Seidman, J. Phys. F: Met. Phys. 3, 393 (1973).

44. D. N. Seidman, K. L. Wilson and C. H. Nielsen, in Proceedings of Fundamental Aspects of Radiation Damage in Metals, edited by M. T. Robinson and F. W. Young, Jr. (National Technical Information Service, Springfield, Virginia, 1975), pp. 373-96.

45. R. M. Scanlan, D. L. Styris and D. N. Seidman, Phil. Mag. 23, 1439 (1971).

46. R. M. Scanlan, D. L. Styris and D. N. Seidman, Phil. Mag. 13, 1459 (1971).

47. K. L. Wilson and D. N. Seidman, Rad. Effects 27, 67 (1975).

48. D. N. Seidman, K. L. Wilson and C. H. Nielsen, Phys. Rev. Lett. 35, 1041 (1975).

49. V. Y. Startsev, N. V. Volkenshteyn and G. A. Nikitina, Fiz. Metal. Metalloved. 26, 261 (1968).

50. F. Dausinger, H. Schultz, K. Bönig, and G. Vogl, Tagungstortrag, Physikertagung in Freudenstadt, April (1974); F. Dausinger and H. Schultz, Phys. Rev. Letter. 35, 1773 (1975).

51. M. Hansen and K. Anderko, Constitution of Binary Alloys; p. 392. McGraw-Hill (1958); E. Fromm and H. Jehn, Met. Trans. 3, 1685 (1972).

52. E. Krautz, H.-H. Kuhlmann and H. Schultz, Z. Metallk. 59, 133 (1968).

53. A. Shepella, Ph.D. Thesis, Cornell University (1970).

54. A. Sosin and H. Neely, Phys. Rev. 127, 1465 (1962).

55. W. Schilling, G. Burger, K. Isebeck and H. Wenzel in Vacancies and Interstitials in Metals, edited by A. Seeger, D. Schumacher, W. Schilling and J. Diehl (North-Holland, Amsterdam, 1970), pp. 255-361.

56. C. H. Nielsen, M. S. thesis, Cornell University (1977).

57. C. H. Nielsen and D. N. Seidman, to be published.

58. D. N. Seidman and K. H. Lie, Acta Met. 20, 1045 (1972).

59. T. J. Wilkes, J. M. Titchmarch, G. D. W. Smith, D. A. Smith, R. F. Morris, S. Johnston, T. J. Godfrey, P. Birdseye, J. Phys. D: Appl. Phys. 5, 2226 (1972).

60. B. Loberg, Phil. Mag. 24, 593 (1971).

61. L. A. Beavan, R. M. Scanlan and D. N. Seidman, Acta Met. 19, 1339 (1971).

62. C.-Y. Wei, Ph.D. Thesis, Cornell University (1978); C.-Y. Wei and D.N. Seidman, Appl. Phys. Lett. 34, 622 (1979).

63. M. Drechsler and P. Wolf in Proc. 4th Int. Cong. Electron Microscopy, (Springer-Verlag, Germany, 1958), Vol. I, p. 835.

64. W. Schilling, P. Ehrhart and K. Sonnenberg in Proceeding of Fundamental Aspects of Radiation Damage in Metals, edited by M. T. Robinson and F. W. Young, Jr. (National Technical Information Service, Springfield, Virginia, 1975), pp. 470-492.

65. R. A. Johnson, Phys. Rev. 134, A1329 (1964).

66. C. W. Gear, Numerical Initial Value Problems in Ordinary Differential Equations (Prentice-Hall, Englewood Cliffs, N. J., 1971).

Table I Chemical Composition of the Various Grades of Tungsten and Tungsten-Rhenium Alloys Employed[†]

Element	Starting Material For Zone-Refining	One-Pass Zone-Refined Tungsten	Four-Pass Zone-Refined Tungsten	Westinghouse Tungsten in The As-Received State	MRC VP Grade Tungsten in The As-Received State	W-0.5 at .% Rhenium	W-3 at .% Rhenium
C	105	*	*	1370	20	*	*
H	*	*	*	*	5	*	*
O	*	*	*	*	25	*	*
N	*	*	*	*	10	*	*
Ag				*	<10		
Al	10-100	0.1-1	1-10	1-10	15	10-100	10-100
As				0.1-1		*	*
Bi	0.3-3			0.1-1		*	*
Ca	10-100	0.1-1	0.1-1		< 5	*	*
Co				0.1-1	<10		
Cr	10-100	1-10	0.1-1	10-100	<15		
Cu					<15		
Fe	10-100	1-10			<15	10-100	10-100
K	10-100	0.1-1	0.1-1			10-100	10-100
Mg	6-60	0.1-1	0.1-1		< 5		
Mn	<0.3	0.1-1	<0.1		< 5		
Mo	1-10			0.1-1	50		
Na		1-10	1-10				
Nb	6-60	0.1-1	0.1-1	*	<15	*	*
P				1-10			
Pb				10-100	<10		
Re		1-10	1-10			10^3-10^4	10^3-10^4
S	0.3-3	*	*	0.1-1		*	*
Si	10-100	10-100	10-100		<10	100-500	100-500
Sn					<10		
Ti	10-100	0.1-1	<0.1	1-10	<10		
V	10-100			1-10			
Zn					<15		

[†]Concentrations are given in atomic parts per million. The MRC VP grade tungsten composition is the typical analysis provided by MRC. All other measurements were made by the Material Science Center Analytical Laboratory of Cornell University. The carbon concentration was measured by the inert gas fusion technique, while the rest of the analyses were obtained from spark source mass spectroscopy. An asterisk (*) indicates that no analysis was made for that element, or that interferences prohibited its detection.

Table II The resistivity ratio (R) for various grades of tungsten used in this experiment.[†]

Type of Specimen	Four-Pass Zone-Refined	One-Pass Zone-Refined	Annealed Westinghouse	Materials Research Corp. (MRC) Very Pure (VP) Grade	Westinghouse Tungsten in the As-Received State	Four-Pass Zone-Refined Tungsten Doped with Carbon	Tungsten-0.5 at .% Rhenium	Tungsten-3 at .% Rhenium
R	$3 \cdot 10^4$ to $5 \cdot 10^4$	$1.5 \cdot 10^4$	50	15	5	250	8.7	2.3
Specimen Diameter (mm)	1.0	1.0	0.125	0.125	0.125	0.2	0.25	0.13

[†]No corrections have been made for the specimen size effect.

Table III A listing of the different types of specimens irradiated, the 30 keV W^+ ion dose, the average tip radius and the number of SIA events observed.

Specimen	Dose ($\times 10^{-12}$ ion cm^{-2})	Radius† (Å)	Number of SIAs Observed
Four Pass Zone-Refined Tungsten [R = (3to5)·10⁴]			
1	20.0	250	15
2A*	9.5	170	6
2B	13.0	220	17
3A	4.5	325	32
3B	4.0	340	39
4A	5.5	325	84
4B	4.5	380	126
One Pass Zone-Refined Tungsten (R=1.5·10⁴)			
1	20.0	230	21
2A	6.6	240	27
2B	5.5	260	35
2C	5.5	275	74
Annealed Westinghouse Tungsten (R=50)			
1A	8.0	300	67
1B	8.0	320	63
1C	6.8	320	82
MRC VP Grade Tungsten (R=15)			
1	25.0	190	12
2	20.0	335	12
3	20.0	250	9
4A	5.6	190	7
4B	20.0	240	7
4C	No measurement	240	5
5	5.4	225	20
6A	5.0	260	45
Westinghouse Tungsten in the As-Received State (R=5)			
1	6.0	230	9
2	6.6	285	19
3A	5.5	265	27
3B	7.0	325	28
4	5.8	330	11
5A	5.0	210	16
5B	8.5	292	44
5C	5.7	325	54
Tungsten -5·10⁻³at.fr. Rhenium (R=8.7)			
1A	3.5	380	17
1B	4.5	380	10
2A	5.5	310	10
2B	6.0	370	25
Tungsten-3·10⁻²at.fr. Rhenium (R=2.3)			
1A	20.0	205	1
1B	50.0	235	1
1C	12.0	235	0
2	20.0	250	1
3A	4.0	315	3
3B	5.0	350	4
Four Pass Zone-Refined Tungsten doped with Carbon (R= 250)			
1A	5.2	190	6
1B	4.6	250	20
2A	5.0	185	16
2B	5.0	230	30
2C	5.0	310	72
Annealed Westinghouse with Carbon			
1	5.0	330	33
2	5.0	280	49
3	5.0	265	15

†Tip radii were measured by the ring counting method of Drechsler and Wolf.[61] An average was taken of the measurements between the 011 and 112 poles.

FIGURE CAPTIONS

Fig. 1. A composite isochronal-annealing spectrum for one-pass zone-refined tungsten irradiated at 18 K with 30 keV W^+ ions to a dose of $5x10^{12}$ ion cm^{-2} and annealed to 120 K at a warming rate of ~2.5 K min^{-1}.

Fig. 2. A composite isochronal annealing spectrum for annealed Westinghouse tungsten irradiated at 18 K with 30 keV $^+$ ions to a dose of $5x10^{12}$ ion cm^{-2} and annealed to 120 K at a warming rate of ~2.5 K min^{-1}.

Fig. 3. A composite isochronal-annealing spectrum for MRC-VP grade tungsten irradiated in the as-received state at 18 K with 30 keV W^+ ions to a dose of $5x10^{12}$ ion cm^{-2} and annealed to 120 K at a warming rate of ~2.5 K min^{-1}.

Fig. 4. A composite isochronal-annealing spectrum for Westinghouse tungsten irradiated in the as-received state irradiated at 18 K with 30 keV W^+ ions and annealed to 120 K at a warming rate of ~2.5 K min^{-1}.

Fig. 5. A composite isochronal-annealing spectrum for four-pass zone-refined tungsten doped with carbon and irradiated at 18 K with 30 keV W^+ ions to a dose of $5x10^{12}$ ion cm^{-2} and then warmed to 120 K at a rate of ~2.5 K min^{-1}.

Fig. 6. A composite isochronal-annealing spectrum for Westinghouse tungsten doped with carbon and irradiated at 18 K with 30 keV W^+ ions to a dose of $5x10^{12}$ ion cm^{-2} and then warmed to 120 K at a rate of ~2.5 K min^{-1}.

Fig. 7.(A): A composite isochronal-annealing spectrum for a tungsten-0.5 at.% rhenium alloy irradiated at 18 K with 30 keV W^+ ions to a dose of $5x10^{12}$ ion cm^{-2} and warmed to 120 K at a rate of ~2.5 K min^{-1}.

(B): A composite isochronal-annealing spectrum for a tungsten-3 at.% rhenium alloy irradiated at 18 K with 30 keV W^+ ion cm^{-2} and warmed to 120 K at a rate of ~2.5 K min^{-1}.

Fig. 8. (A) and (B): The appearance of a double-spot SIA contrast pattern detected in the (110) terraces at 42.0 K during an isochronal anneal.

(C) and (D): The appearance of another double-spot SIA contrast pattern in the (110) terraces at 54.0 K during an isochronal anneal.

(E) and (F): The appearance of a multiple-spot SIA contrast pattern near the (210) plane at 50.0 K during an isochronal anneal.

(G) and (H): The appearance of a multiple-spot SIA contrast pattern near the (112) plane at 64.5 K during an isochronal anneal. The entire surface is seen to change dramatically in this region for this particular event.

In all four cases the micrographs recorded before and after the appearance of the SIA were taken 2.0 sec apart, which corresponds to a temperature interval of ~0.08 K.

Fig. 9. A plot of the fraction of SIAs that were trapped during Stage I and the fraction of SIAs that had escaped to the outer surface during Stage I as a function of the impurity-atom concentration. These results were obtained by solving the set of coupled non-linear partial differential equations that governed the situation; see Appendix for further details.

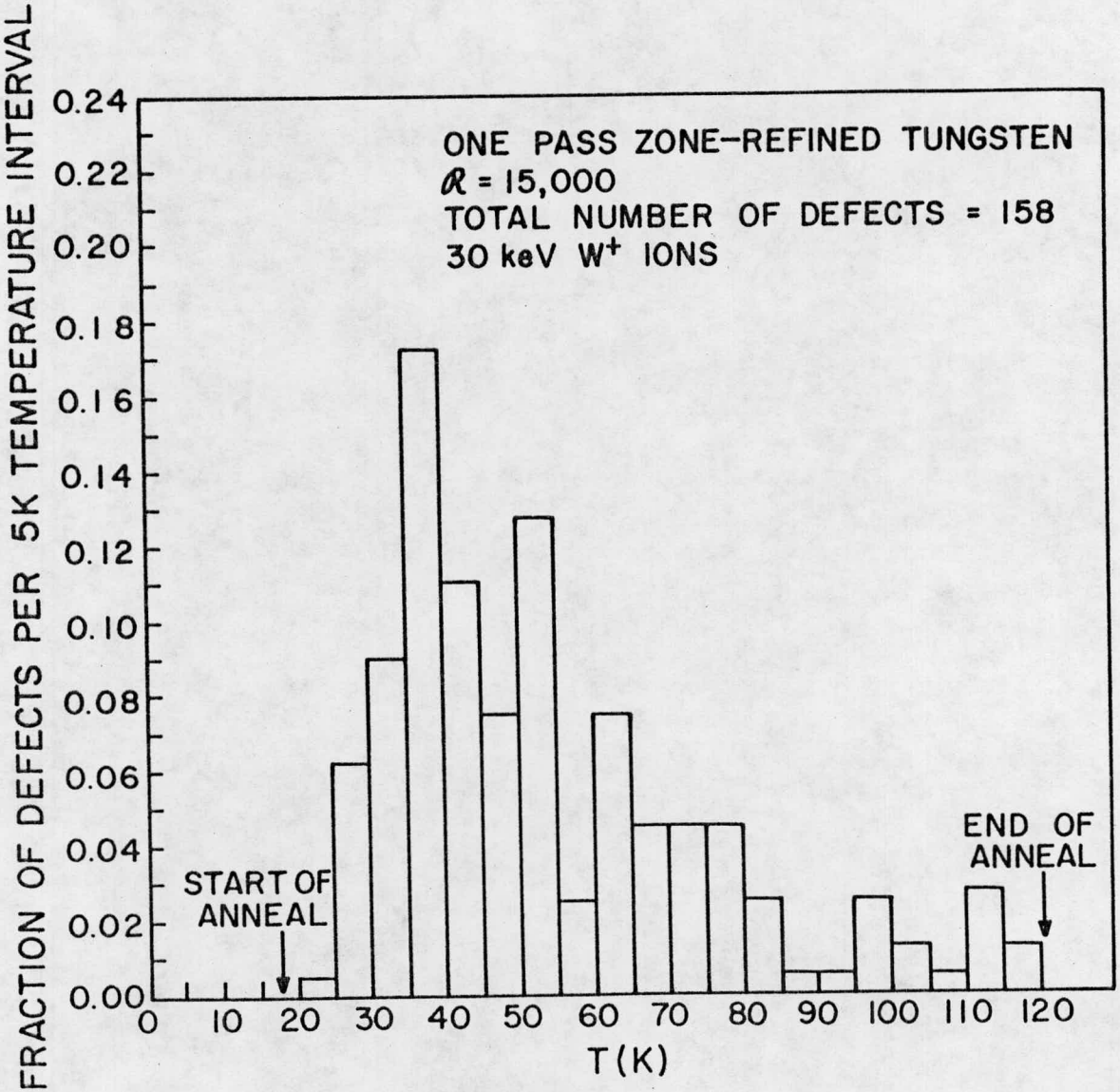
ONE PASS ZONE-REFINED TUNGSTEN
ℛ = 15,000
TOTAL NUMBER OF DEFECTS = 158
30 keV W+ IONS
FRACTION OF DEFECTS PER 5K TEMPERATURE INTERVAL
0.24
0.22
0.20
0.18
0.16
0.14
0.12
0.10
0.08
0.06
0.04
0.02
0.00
START OF ANNEAL
END OF ANNEAL
0 10 20 30 40 50 60 70 80 90 100 110 120
T(K)

Figure 1

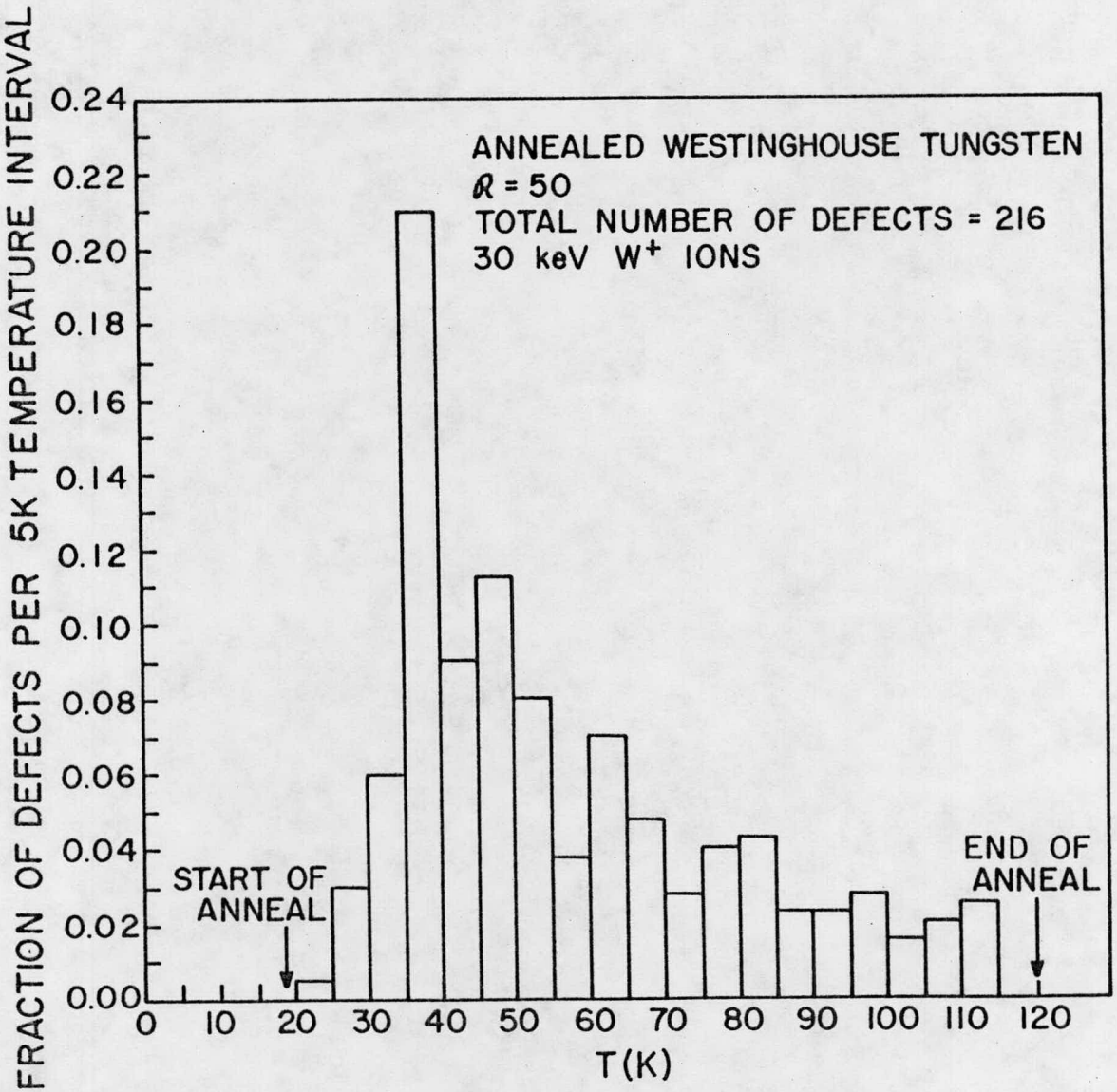
ANNEALED WESTINGHOUSE TUNGSTEN
R = 50
TOTAL NUMBER OF DEFECTS = 216
30 keV W+ IONS
FRACTION OF DEFECTS PER 5K TEMPERATURE INTERVAL
0.24
0.22
0.20
0.18
0.16
0.14
0.12
0.10
0.08
0.06
0.04
0.02
0.00
START OF ANNEAL
END OF ANNEAL
0 10 20 30 40 50 60 70 80 90 100 110 120
T(K)

Figure 2

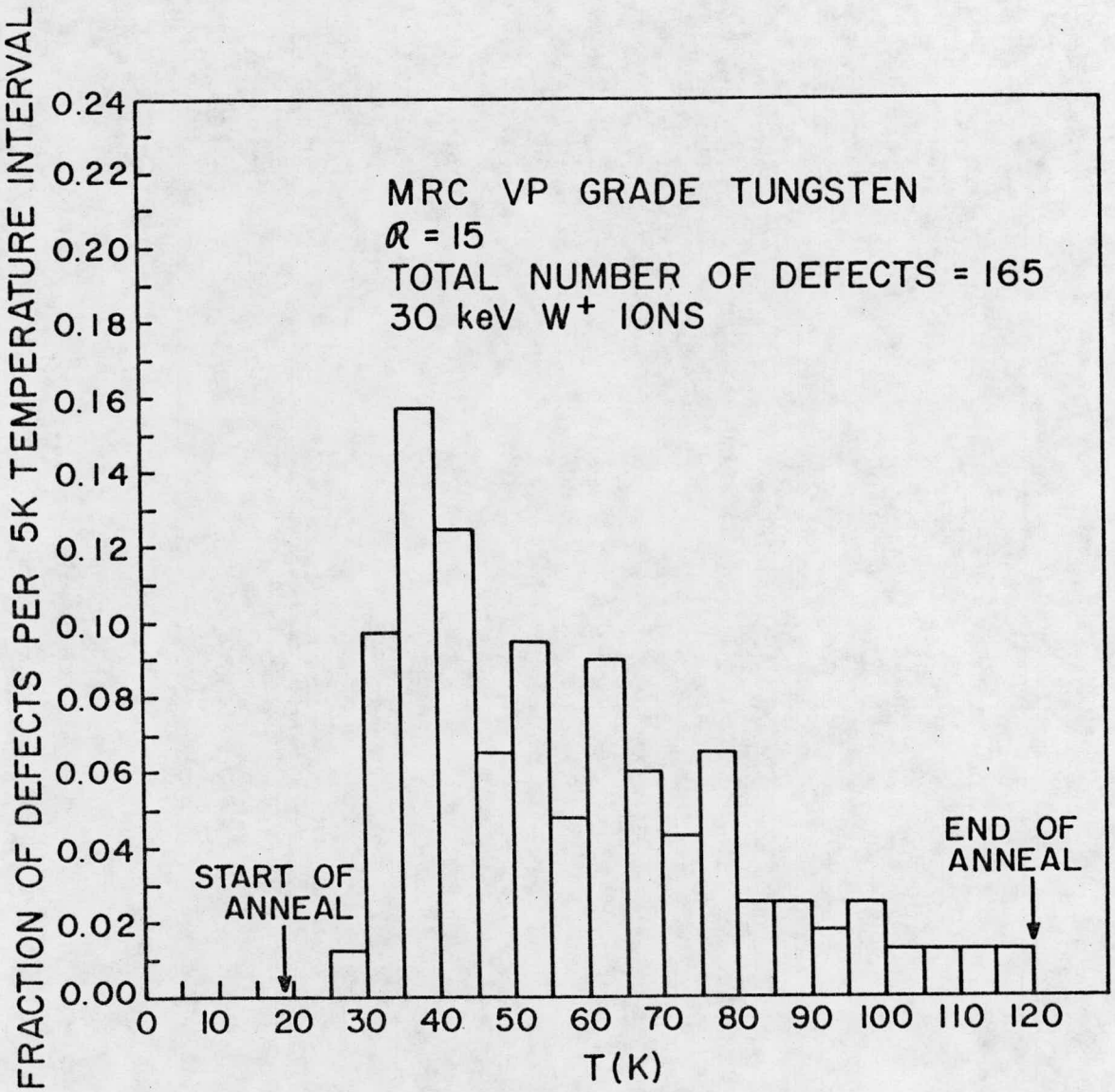
FRACTION OF DEFECTS PER 5K TEMPERATURE INTERVAL
0.24
0.22
0.20
0.18
0.16
0.14
0.12
0.10
0.08
0.06
0.04
0.02
0.00
MRC VP GRADE TUNGSTEN
R = 15
TOTAL NUMBER OF DEFECTS = 165
30 keV W+ IONS
START OF ANNEAL
END OF ANNEAL
0 10 20 30 40 50 60 70 80 90 100 110 120
T(K)

Figure 3

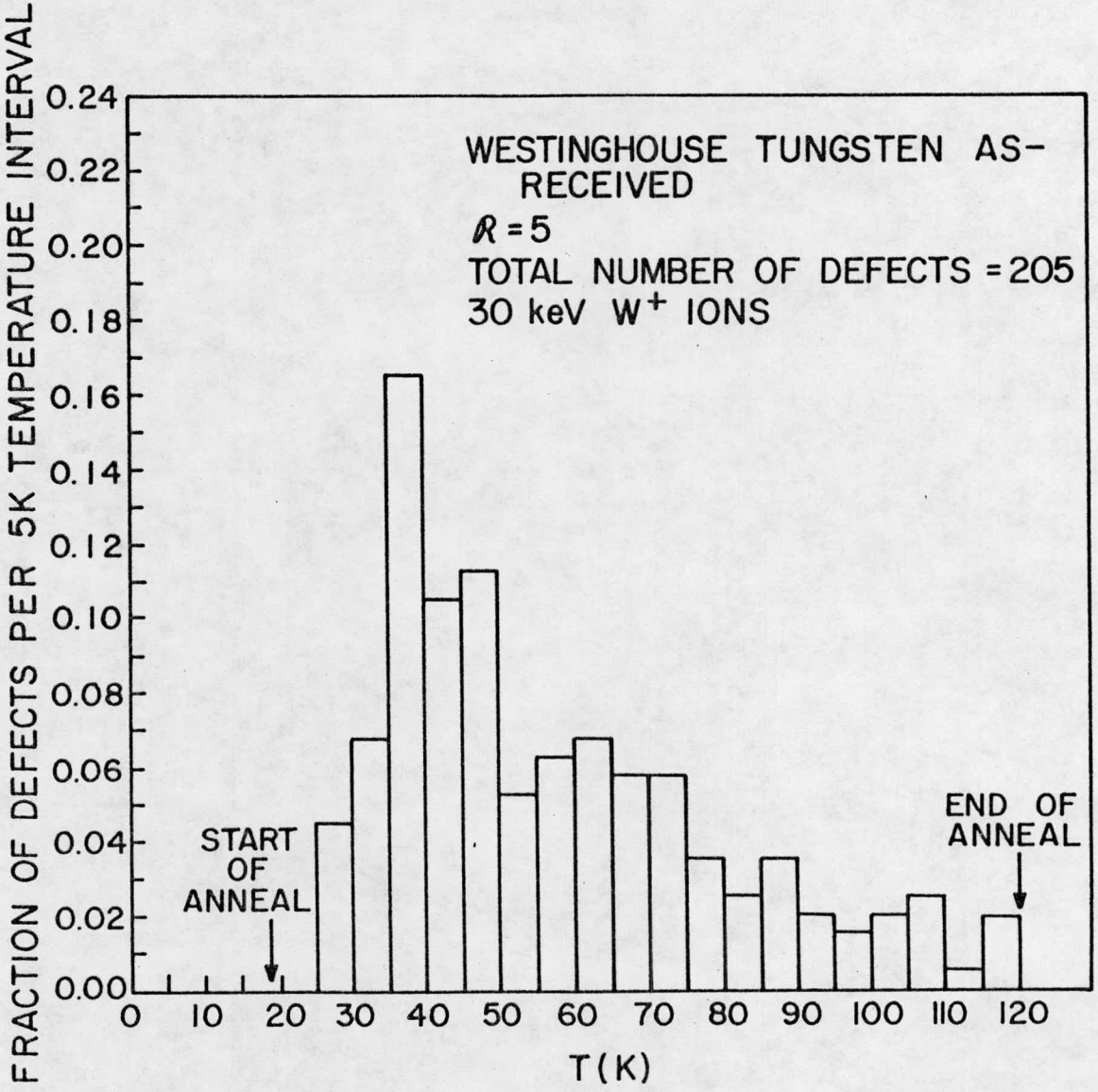
WESTINGHOUSE TUNGSTEN AS-RECEIVED
R = 5
TOTAL NUMBER OF DEFECTS = 205
30 keV W+ IONS
START OF ANNEAL
END OF ANNEAL
FRACTION OF DEFECTS PER 5K TEMPERATURE INTERVAL
0.24
0.22
0.20
0.18
0.16
0.14
0.12
0.10
0.08
0.06
0.04
0.02
0.00
0 10 20 30 40 50 60 70 80 90 100 110 120
T(K)

Figure 4

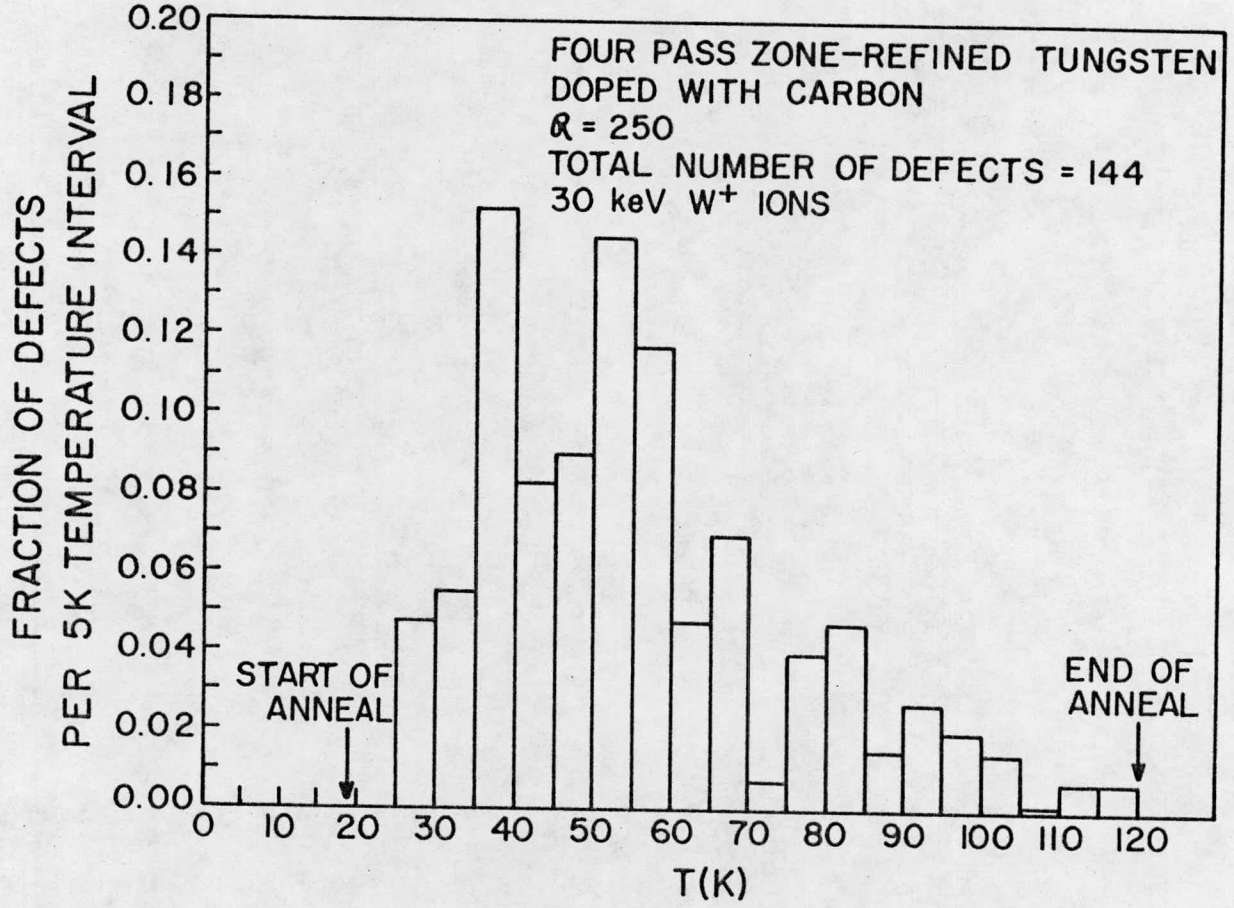
FOUR PASS ZONE-REFINED TUNGSTEN
DOPED WITH CARBON
R = 250
TOTAL NUMBER OF DEFECTS = 144
30 keV W+ IONS
FRACTION OF DEFECTS
PER 5K TEMPERATURE INTERVAL
0.20
0.18
0.16
0.14
0.12
0.10
0.08
0.06
0.04
0.02
0.00
START OF
ANNEAL
END OF
ANNEAL
0
10
20
30
40
50
60
70
80
90
100
110
120
T(K)

Figure 5

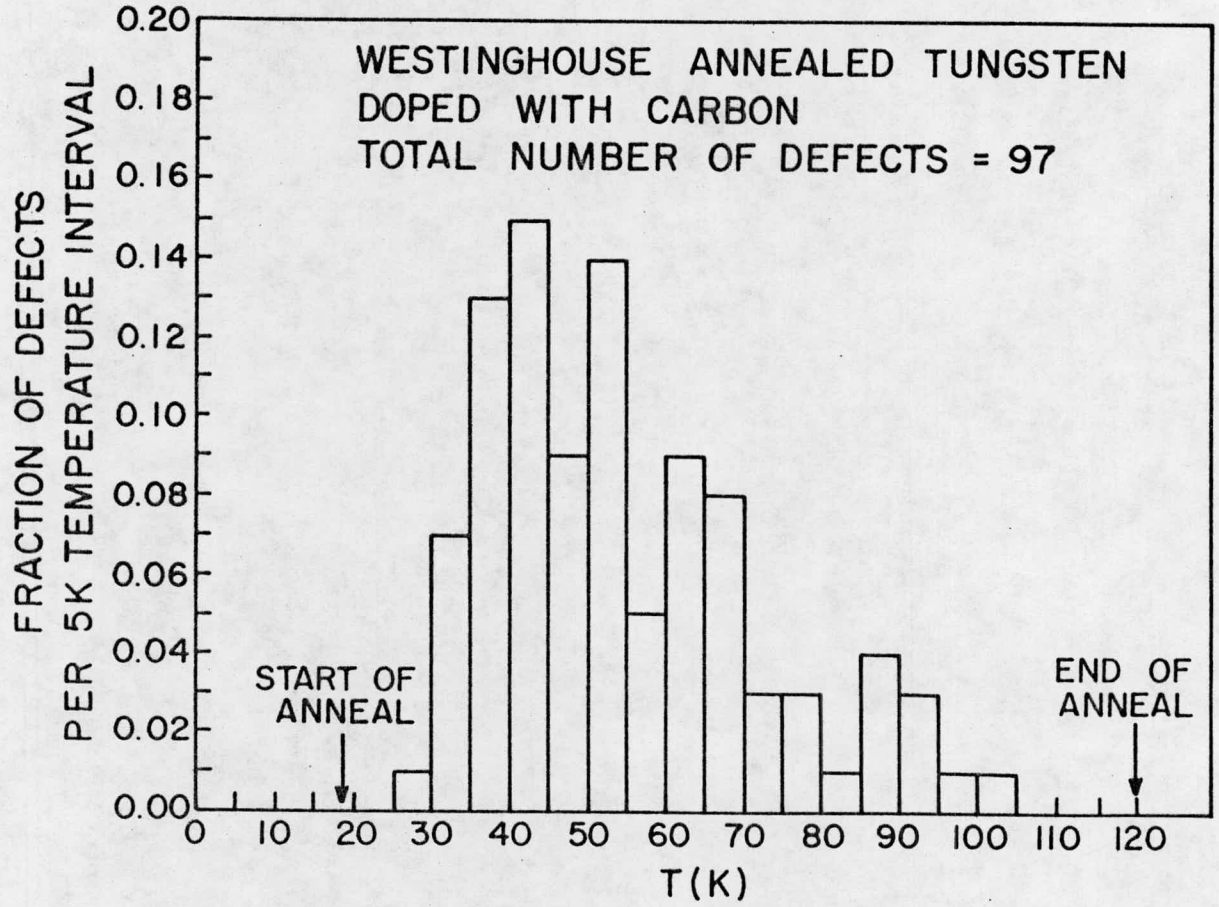
WESTINGHOUSE ANNEALED TUNGSTEN
DOPED WITH CARBON
TOTAL NUMBER OF DEFECTS = 97
FRACTION OF DEFECTS
PER 5K TEMPERATURE INTERVAL
0.20
0.18
0.16
0.14
0.12
0.10
0.08
0.06
0.04
0.02
0.00
START OF
ANNEAL
END OF
ANNEAL
0
10
20
30
40
50
60
70
80
90
100
110
120
T(K)

Figure 6

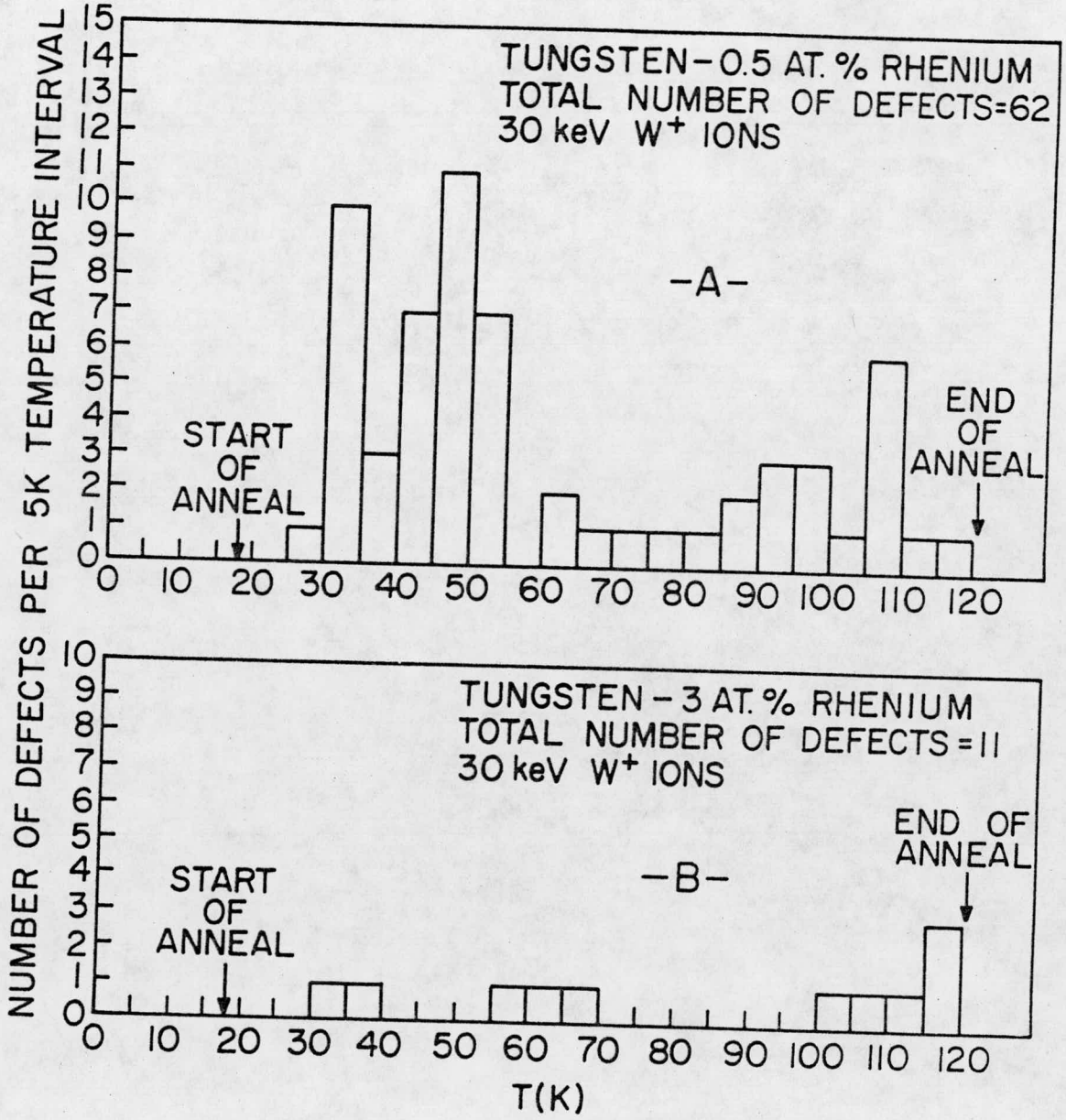
TUNGSTEN – 0.5 AT. % RHENIUM
TOTAL NUMBER OF DEFECTS=62
30 keV W+ IONS
-A-
START OF ANNEAL
END OF ANNEAL
TUNGSTEN – 3 AT. % RHENIUM
TOTAL NUMBER OF DEFECTS = 11
30 keV W+ IONS
-B-
START OF ANNEAL
END OF ANNEAL
NUMBER OF DEFECTS PER 5K TEMPERATURE INTERVAL
T(K)

Figure 7

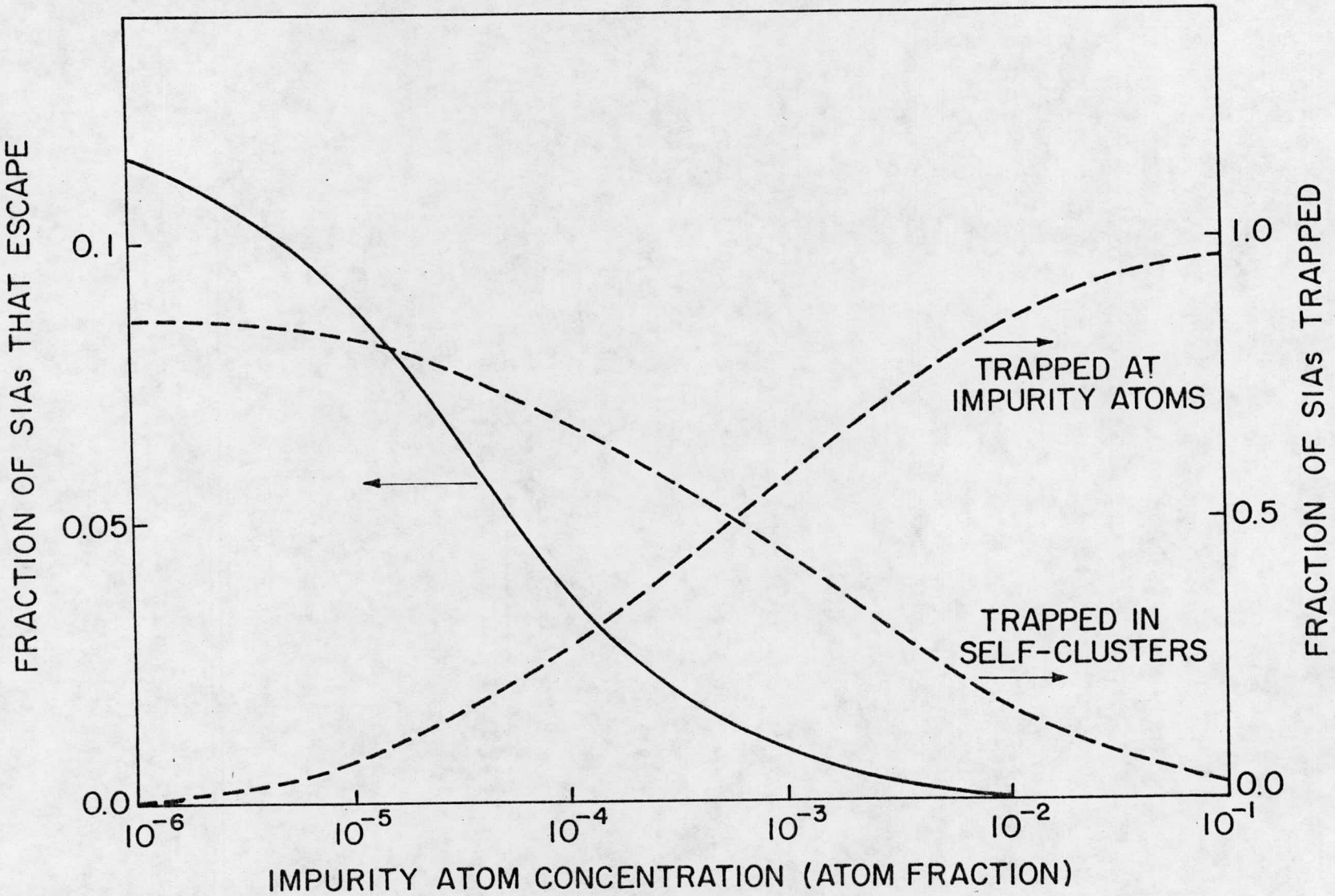
FRACTION OF SIAs THAT ESCAPE
0.1
0.05
0.0
1.0
0.5
0.0
FRACTION OF SIAs TRAPPED
TRAPPED AT IMPURITY ATOMS
TRAPPED IN SELF-CLUSTERS
10^{-6}
10^{-5}
10^{-4}
10^{-3}
10^{-2}
10^{-1}
IMPURITY ATOM CONCENTRATION (ATOM FRACTION)

Figure 8

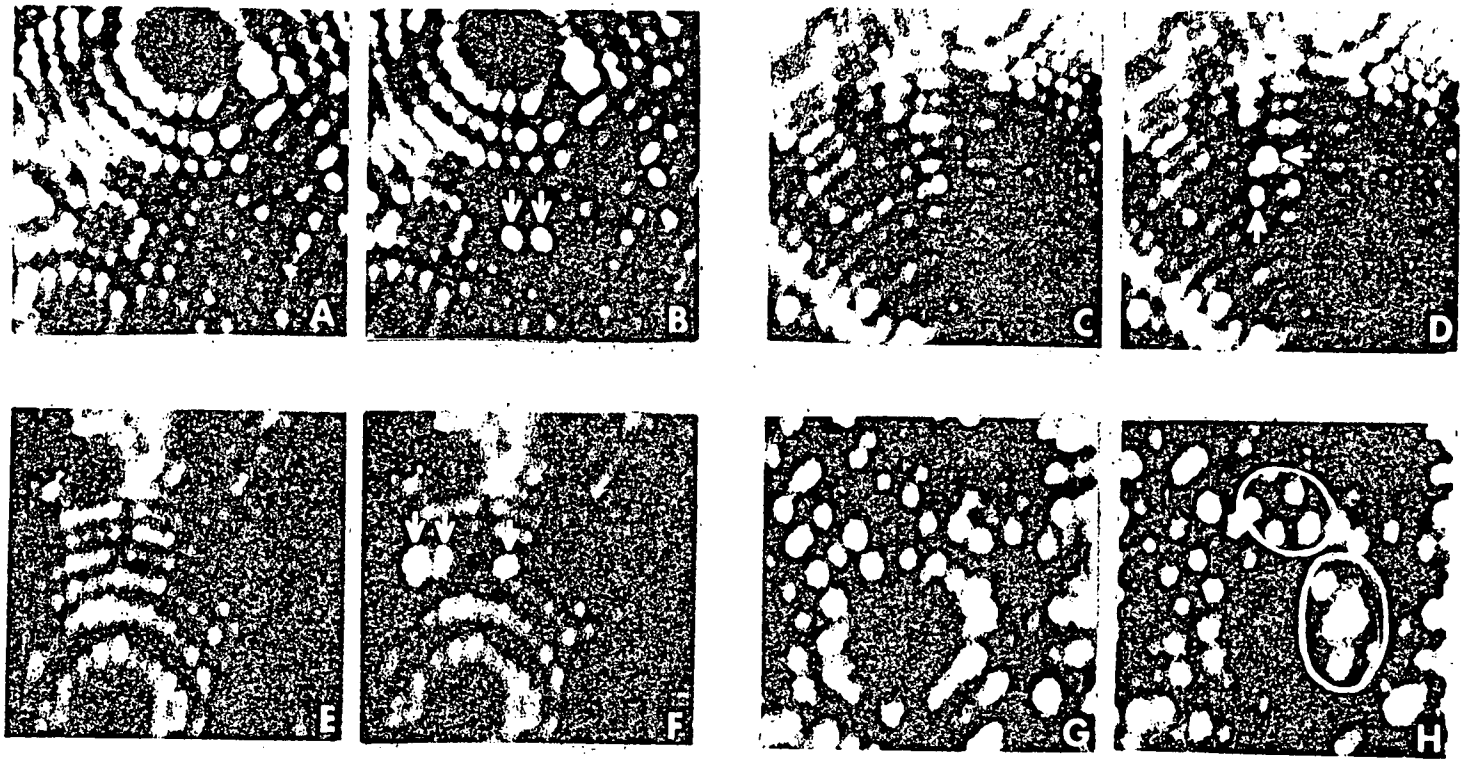

Figure 9